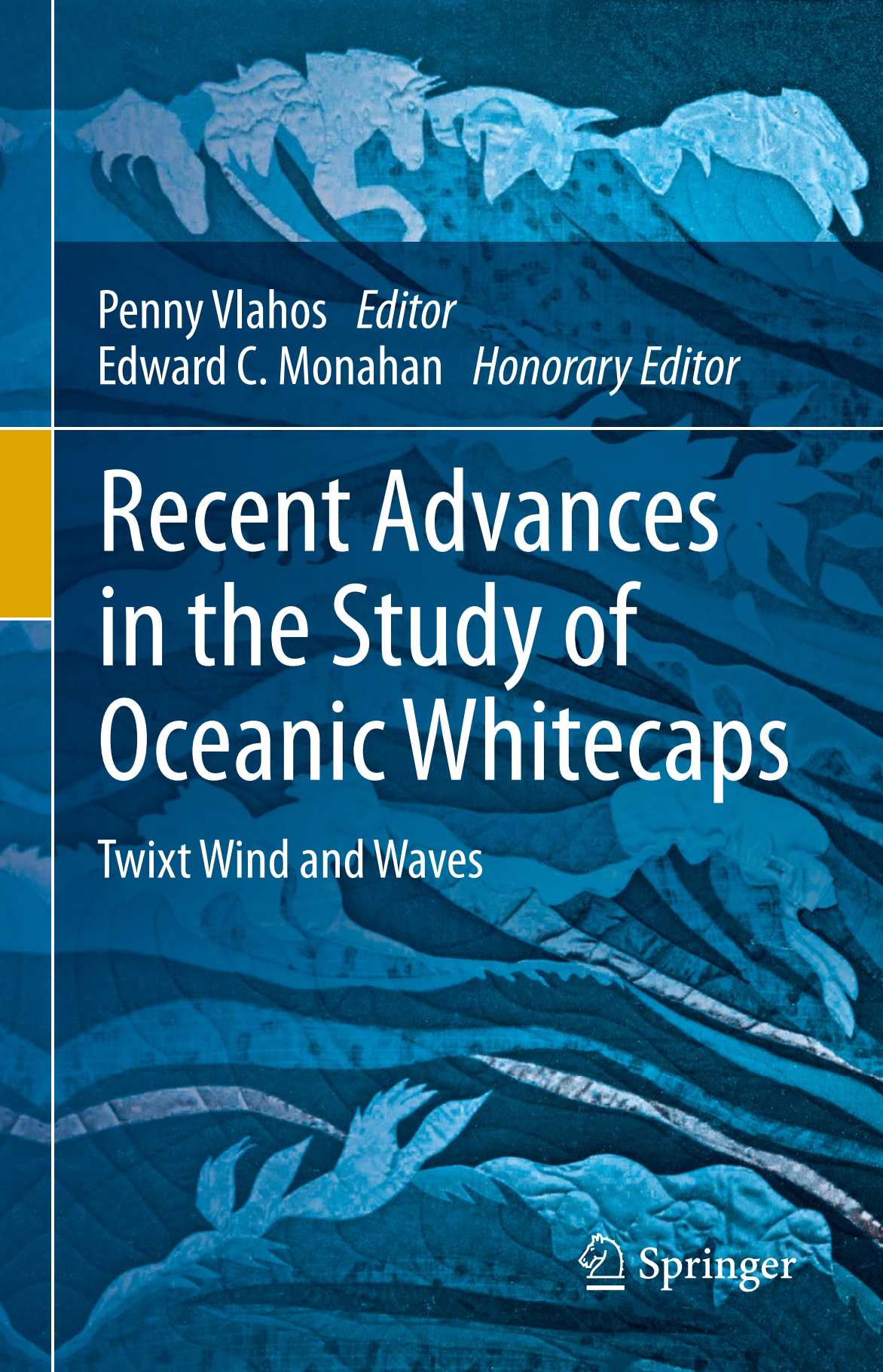
Penny Vlahos Editor
Edward C. Monahan Honorary Editor
Recent Advances in the Study of Oceanic Whitecaps
Twixt Wind and Waves
Springer

Editor
Penny Vlahos
Department of Marine Sciences
University of Connecticut
Groton, CT, USA

Honorary Editor
Edward C. Monahan
Department of Marine Sciences
University of Connecticut
Groton, CT, USA

ISBN 978-3-030-36370-3 ISBN 978-3-030-36371-0 (eBook)
https://doi.org/10.1007/978-3-030-36371-0

This Springer imprint is published by the registered company Springer Nature Switzerland AG.
The registered company address is: Gewerbestrasse 11, 6330 Cham, Switzerland

Contents

Chapter 11
Global Whitecap Coverage from Satellite Remote Sensing and Wave Modelling

Magdalena D. Anguelova

Abstract For decades, photographic measurements of whitecap coverage W have been the workhorse for characterizing oceanic whitecaps and parameterizing air-sea processes associated with them. The detail that in situ W data provide is now complemented with the possibilities offered by long-term, consistent determination of W on a global scale from passive microwave remote sensing and from third generation wave modelling. This chapter gives an overview of the development and present status of obtaining the whitecap fraction with remote sensing and wave models.

11.1 Introduction

Global whitecap fraction (or coverage) W can be useful to evaluate more accurately the air-sea surface fluxes of momentum, mass, and energy under a variety of environmental conditions. Reliable assessment of air-sea fluxes is necessary to reproduce more realistically the coupling between the ocean and the atmosphere in numerical weather prediction, chemical transport, and climate models. Usually, computations of global surface fluxes use maps of global whitecap fraction obtained with parameterizations of W as a function of wind speed at a reference height of 10 m above the surface, U_{10}. Numerous $W(U_{10})$ parameterizations exist (Anguelova and Webster 2006; Goddijn-Murphy et al. 2011; Brumer et al. 2017). These are based on in situ (most often shipboard) measurements of U_{10} collected together with photographs of the sea state. Image processing algorithms, involving the choice of an intensity threshold, have been used to extract W from such sea state photographs; see Chap. 2 for details on the photographic method of measuring W.

The exponents of the wind speed dependences in existing $W(U_{10})$ parameterizations vary widely, reflecting local meteorological and oceanographic (hereafter metoc) conditions. Predictions of W with such in situ $W(U_{10})$ parameterizations differ when using U_{10} values from either shipboard data sets, or satellite retrievals, or

M. D. Anguelova (✉)
Remote Sensing Division, Naval Research Laboratory, Washington, DC, USA
e-mail: maggie.anguelova@nrl.navy.mil

P. Vlahos (ed.), *Recent Advances in the Study of Oceanic Whitecaps*,
https://doi.org/10.1007/978-3-030-36371-0_11

numerical models (Goddijn-Murphy et al. 2011; Paget et al. 2015). This implies that the accuracy of global surface fluxes would depend on the choice of the $W(U_{10})$ expression and the source of the U_{10} values.

In addition, individual in situ data sets are not sufficient to support the development of parameterizations predicting the natural variability of whitecap formation, whitecap spatial extent, and whitecap temporal evolution. Each in situ data set represents a limited range of metoc conditions, which hinders the quantification of whitecap dependences beyond that on the wind speed. Compilations of in situ data sets, representative of different experimental sites, had partially alleviated this situation in the past. For example, Monahan and O'Muirchaertaigh (1980) used two data sets to develop the widely used expression $W(U_{10})$ with wind exponent of 3.41. Five in situ data sets enabled Monahan and O'Muirchaertaigh (1986) to clearly demonstrate the dependence of whitecap inception on the sea surface temperature (SST) T and to quantify W in terms of both U_{10} and atmospheric stability ΔT (defined as the difference between SST and air temperature T_a, $\Delta T = T - T_a$). The inclusion of additional dependences in W parametrizations—e.g., those of the wave field and/or the influence of salinity and surface active materials (surfactants)—can help to predict the spread of the W data due to the natural whitecap variability.

However, differences caused by equipment, measuring protocols, and subsequent image processing continue to contribute to the spread of measured or predicted W values based on a medley of photographic data sets (Paget et al. 2015). In short, while in situ field campaigns provide valuable data for detail studies of air-sea processes in different metoc environments, the in situ W data are not sufficient to develop new $W(U_{10}, etc.)$ parameterizations applicable on a global scale.

The desire to minimize the spread of W data associated with difficulties of the photographic method, and the need to predict adequately the natural whitecap variability, led to efforts in the last 15 or so years to develop different methods for measuring whitecap fraction. These methods involve remote sensing and wave models. Both methods have the potential to provide consistent, long-term W data sets covering the global range of metoc conditions. Compiling a database of global W data and additional metoc variables can supply sufficient data to study and quantify the natural whitecap variability. This chapter gives an overview of the development and present status of obtaining whitecap fraction with remote sensing and wave models.

11.2 Satellite Remote Sensing of Whitecap Fraction

Satellite remote sensing is an obvious choice for obtaining global whitecap fraction. Satellite-based observations can provide longstanding daily measurements of whitecaps and controlling (forcing) metoc variables such as wind speed U_{10}, significant wave height H_s, SST T, air temperature T_a, salinity S, and surfactant proxies (e.g., ocean color or primary production). Especially valuable are routine observations from a single satellite platform because simultaneous, collocated measurements of

W and other variables would minimize the spread among data points caused by spatial and temporal mismatch.

Oceanic whitecaps have distinct remote sensing signatures in different regions of the electromagnetic (EM) spectrum, each with specific pros and cons; refer to de Leeuw et al. (2011) for a brief review. The high reflectivity of the sea foam is the basis for whitecap observations at visible wavelengths, including the use of still photographs and video images (Monahan 1971; Bobak et al. 2011). Only recently the photographic method was complimented with a novel method inferring whitecap fraction from the total upwelling radiance measured with a radiometer at visible (411 nm) wavelengths (Randolph et al. 2017).

Observations of breaking waves and surface renewal at infrared (IR) wavelengths have been available for some time (Jessup et al. 1997). Observing and quantifying whitecap properties at IR wavelengths is a recent development. Potter et al. (2015) demonstrated the unique use of IR cameras for whitecap observations. The presence of relatively strong signals in the IR region of the EM spectrum from both actively breaking waves and decaying foam patches allows to quantify the lifetimes of stage A (active, young) and stage B (residual, mature) whitecaps (as defined by Monahan and Lu 1990).

Microwave radiometry is a suitable observational tool of whitecaps due to the high, black-body-like emissivity of sea foam at microwave wavelengths with frequencies of 1–37 GHz (Anguelova and Gaiser 2012). The tractability of removing the atmospheric influence on the signals emanated from whitecaps on the ocean surface is a good justification for satellite-based radiometric observations of W. The relatively low spatial resolution of the satellite observations at microwave frequencies is somewhat compensated by the consideration that microwave radiometers provide statistical (spatially averaged) measure of whitecap fraction, a provision fitting well the stochastic nature of breaking waves (Bondur and Sharkov 1982; Melville and Matusov 2002; Mironov and Dulov 2008). This section summarizes the status of using microwave radiometry to obtain the whitecap fraction from satellite observations.

11.2.1 Microwave Ocean Emissivity and Whitecaps

The microwave remote sensing signature of the whitecaps is related to variations of the natural ocean thermal emission e occurring when wind waves break and produce sea foam. Brightness temperature $T_B = eT$ quantifies the natural ocean thermal emission at microwave frequencies for a given SST. The strong relationship between T_B and the sea foam emissivity is the physical basis for estimating W from satellite microwave observations. The relationship $T_B(W)$ has been established by a long history of passive microwave measurements (see Bobak et al. 2011 and the references there-in). Williams (1969) first measured T_B variations in presence of foam (along with T_B of flat and rough surfaces) and proposed explanation of the high foam emissivity. Subsequent measurements at different microwave frequencies confirmed

the high foam emissivity leading to large variations of T_B (Nordberg et al. 1971; Ross and Cardone 1974; Militskii et al. 1978; Smith 1988; Rose et al. 2002; Padmanabhan et al. 2006).

The remote sensing community saw great opportunity in using the effect of sea foam (and roughness) on T_B for microwave sensing of the ocean, especially for retrieving wind speed U_{10}. The development of geophysical retrieval algorithms required modeling of the emissivity e and T_B of rough (Stogryn 1967; Wentz 1975) and foamy (Droppleman 1970; Stogryn 1972) surfaces. These efforts yielded the first inference of whitecap fraction W using T_B data from the Scanning Multichannel Microwave Radiometer (SMMR) (Pandey and Kakar 1982; Wentz 1983). As the geophysical retrieval algorithms matured, it became clear that it is sufficient to include the sea foam signal only implicitly in wind-induced terms (Wentz 1997; Bettenhausen et al. 2006; Meissner and Wentz 2012). Such representation of sea foam contribution to the T_B registered by a satellite radiometer is valid when we do not seek to retrieve whitecap fraction.

The seminal paper of Monahan and O'Muircheartaigh (1986) introduced the connection between W and the passive remote sensing of the ocean surface to the air-sea interaction community. The Monahan and O'Muircheartaigh (1986) analysis clearly justified the need to account for additional variables when relating T_B, U_{10}, and W. Measurements of T_B and W in a surf pool during the Wave Basin Experiment in October 1993 (WABEX-93) were the first to quantify an air-sea process (namely, air-water gas transfer) using microwave radiometry (Asher et al. 1995). The observed correlation between W and T_B at horizontal (H) and vertical (V) polarizations enabled the derivation of empirical expressions for the gas transfer velocity in terms of measured T_B (Wang et al. 1995). Further analysis by Asher et al. (1998) showed that microwave radiometric data have the necessary precision to obtain gas transfer velocities.

Building on these previous efforts from both the remote sensing and the air-sea interaction communities, Anguelova and Webster (2006) renewed attempts to infer whitecap fraction W from satellite T_B observations. They proved the feasibility of satellite remote sensing of W by using T_Bs from the Special Sensor Microwave Imager (SSM/I).

11.2.2 Passive Remote Sensing of Whitecaps

The concept of an algorithm obtaining whitecap fraction W from satellite measurements of ocean brightness temperature T_B, hereafter referred to as $W(T_B)$ algorithm, has been given in detail by Anguelova and Webster (2006) and Anguelova and Bettenhausen (2019). It is briefly summarized here.

We seek to develop a physical $W(T_B)$ algorithm because it allows to account for processes associated with breaking waves and whitecaps better than empirical expressions do. Physical $W(T_B)$ algorithm must be based on a radiative transfer model (RTM) in order to properly couple air-sea processes with atmospheric

propagation effects. The RTM gives the T_B at the top of the atmosphere (TOA) with four terms:

$$T_{Bp}^{\mathrm{TOA}} = \tau e_p T + T_{BU} + \tau \Omega_{Dp} r_p T_{BD} + \tau^2 \Omega_{Cp} r_p T_C \tag{11.1}$$

where p refers to polarization (H or V) (hereafter omitted for simplicity). The first term in (11.1) is the brightness temperature of a sea surface with emissivity e at SST T. The remaining three terms represent contributions from the atmosphere, namely upwelling and downwelling atmospheric radiation, T_{BU} and T_{BD}, and cosmic background radiation T_C. Reflectivity $r = 1 - e$ represents the reflection of T_{BD} and T_C from the ocean surface back to space. The atmospheric transmissivity τ accounts for the attenuation of the microwave radiation as it propagates up and down through the atmosphere. The Ω factors in the T_{BD} and T_C terms account for their non-specular (diffuse) reflection from a rough sea surface.

Variables e and r in (11.1) carry the information for whitecap fraction W. The surface emissivity e comprises two contributions: emissivity of rough surface e_r and emissivity of whitecaps e_W. Whitecap fraction W controls the relative contributions of terms e_r and e_W to T_B^{TOA} in (11.1). The following equation expresses this premise:

$$e = e_r + e_W = (1 - W)E_r + WE_f \tag{11.2}$$

with E_r being the emissivity of rough, foam-free sea surface and E_f the emissivity of 100% foam-covered sea surface.

Equation (11.2) offers different approaches to obtaining W. Anguelova and Webster (2006) obtained whitecap fraction by solving (11.2) for variable W:

$$W = \frac{e - E_r}{E_f - E_r} \tag{11.3}$$

Anguelova and Bettenhausen (2019) solve (11.2) for the whitecap term:

$$e_W = e - e_r = e - (1 - W)E_r = WE_f. \tag{11.4}$$

From (11.4), Anguelova and Bettenhausen (2019) obtain W as:

$$W = e_W / E_f = (e - e_r)/E_f. \tag{11.5}$$

The composite (roughness + foam) and the roughness-only emissivity terms e and e_r in (11.2, 11.3, 11.4 and 11.5) are obtained by solving (11.1) for the respective sea surface emissivity:

$$e = \left(T_B^{\mathrm{TOA}} - B\right)/A \tag{11.6a}$$

$$e_r = \left(T_{Br}^{\mathrm{TOA}} - B\right)/A \tag{11.6b}$$

where

$$A = \tau(T - \Omega_D T_{BD} - \tau\Omega_C T_C) \tag{11.7a}$$

$$B = T_{BU} + \tau\Omega_D T_{BD} + \tau^2\Omega_C T_C. \tag{11.7b}$$

In (11.3) and (11.5), terms e and e_r are corrected for the atmospheric signal with factors A and B, thus providing W at the surface. Both measured and modeled data are necessary to obtain W with (11.3) or (11.5). The specific choices of data and models lead to different implementations of the $W(T_B)$ algorithm.

11.2.3 Implementations of the $\mathbf{W(T_B)}$ Algorithm

Several models are necessary to calculate T_B^{TOA} and T_{Br}^{TOA} in (11.6) with (11.1) and (11.2). An atmospheric model provides the atmospheric variables τ, T_{BU}, and T_{BD}. Models for surface roughness and wave spectrum are necessary for e_r or E_r. A model for the foam emissivity is needed for E_f . We need both instrumental (sensor) and geophysical variables to run these models. The sensor variables include the radiometer frequency f, polarization p, and Earth incidence angle θ. The geophysical variables necessary for the atmospheric model are water vapor V, cloud liquid water L, and SST T. The model for the foam emissivity needs data for T and S. The roughness model, through the wave spectrum, needs data for T, θ, U_{10}, and wind direction. The input variables forcing the models can be geophysical retrievals from different satellites and/or data from numerical models.

Anguelova and Webster (2006) combined simple and empirical models with satellite data to calculate the emissivities in (11.3). They simplified the RTM by assuming specular reflection of T_B from a flat sea surface and setting the Ω factors in (11.1) to 1. Empirical expressions were used to calculate E_r. Foam emissivity E_f was computed from foam reflectivity R_f, which, in turn, was computed with the Fresnel formula using foam permittivity ε_f calculated from the Maxwell Garnett formula (Anguelova 2008) with a constant void fraction. The composite surface emissivity e, corrected for the atmospheric signal as in (11.6a), was obtained from SSM/I observations of T_B at 19.35 GHz. SSM/I retrievals of U_{10}, V, and L were used as input to the chosen models. Anguelova and Webster (2006) suggested two major improvements to further develop the $W(T_B)$ algorithm. These were: (i) Use of physical (instead of empirical and simple) models for rough and foam-covered sea surfaces; and (ii) Use of independent data as input to those models. The decoupling of the sources for T_B and the model inputs aims to avoid intrinsic correlations between the emissivities in (11.3) or (11.5).

Anguelova and Bettenhausen (2019) realized these two suggestions within the framework of the WindSat mission (Gaiser et al. 2004). In pursuing the use of

physical models, Anguelova and Bettenhausen (2019) implemented the $W(T_B)$ algorithm with (11.5) using three notable changes in the modeling. First, they accounted for the non-specular reflections from the ocean surface by including the Ω factors in the RTM (11.1). Second, they used the so-called 2-scale model for the roughness-only term e_r instead of empirical expressions (Bettenhausen et al. 2006). Third, a dedicated foam emissivity RTM was developed for E_f (Anguelova and Gaiser 2013). In pursuing the use of independent data sets as inputs to those models, Anguelova and Bettenhausen (2019) combined WindSat T_B observations for the composite term e with independent geophysical variables (matched in time and space with WinSat T_Bs) to force the roughness and foam models. Specifically, an early (interim) version of the $W(T_B)$ algorithm used wind vector (speed and direction) from QuikSCAT, V and L from SSM/I on platform f13, and SST from NCEP/GDAS (Global Data Assimilation System of the National Centers for Environmental Prediction).

Anguelova and Bettenhausen (2019) show that the interim version of the $W(T_B)$ algorithm produced noisy satellite-based W data mostly due to space-time mismatch of WindSat and external data. Efforts to minimize the spread of the W data yielded a modified version of the interim algorithm, which did not use the WindSat T_Bs observations directly for the composite term e. Rather, the $W(T_B)$ algorithm employed a semi-empirical model for e, which was developed on the basis of WinSat T_Bs (Bettenhausen et al. 2006). This trade-off between W computations using either independent data (to avoid intrinsic correlations of emissivity terms) or direct Windat T_B observations (to avoid spread of W data from collocation) prompted the consideration of an algorithm version with fewer data sources. Disruptions in the availability of external data (e.g., SSM/I on f13 and QuikSCAT failed in 2009) further supported this idea. As a result, an updated (and currently the latest) version of the $W(T_B)$ algorithm uses the WindSat T_Bs for term e in (11.5) and the WindSat geophysical retrievals (T, V, L, U_{10}, and wind direction) for the terms e_r and e_W.

11.2.4 Satellite Whitecap Fraction

The latest (updated) version of the $W(T_B)$ algorithm (Sect. 11.2.3) retrieves whitecap fraction W at four WindSat frequencies, from 10 to 37 GHz, and H and V polarizations. Figure 11.1 shows W retrievals as a function of wind speed U_{10}. Panel a shows W from T_B at 18 GHz, H and V polarizations (squares and asterisks, respectively) in logarithmic scale along the y-axis. The W values at V polarization are lower than the W values at H polarization by a factor of 2–3 depending on the frequency. Panel b shows the wind speed dependence of W retrievals for H polarization at frequencies of 10, 18, and 37 GHz (triangles, squares, and diamonds, respectively) in linear scales. In contrast to the W retrievals at H polarization (Fig. 11.1b), the W values at V polarization differ little for different frequencies (not shown). The satellite W values are compared in Fig. 11.1 to W values from the $W(U_{10})$ parametrization of Monahan and O'Muirchaertaigh (1980) (gray symbols).

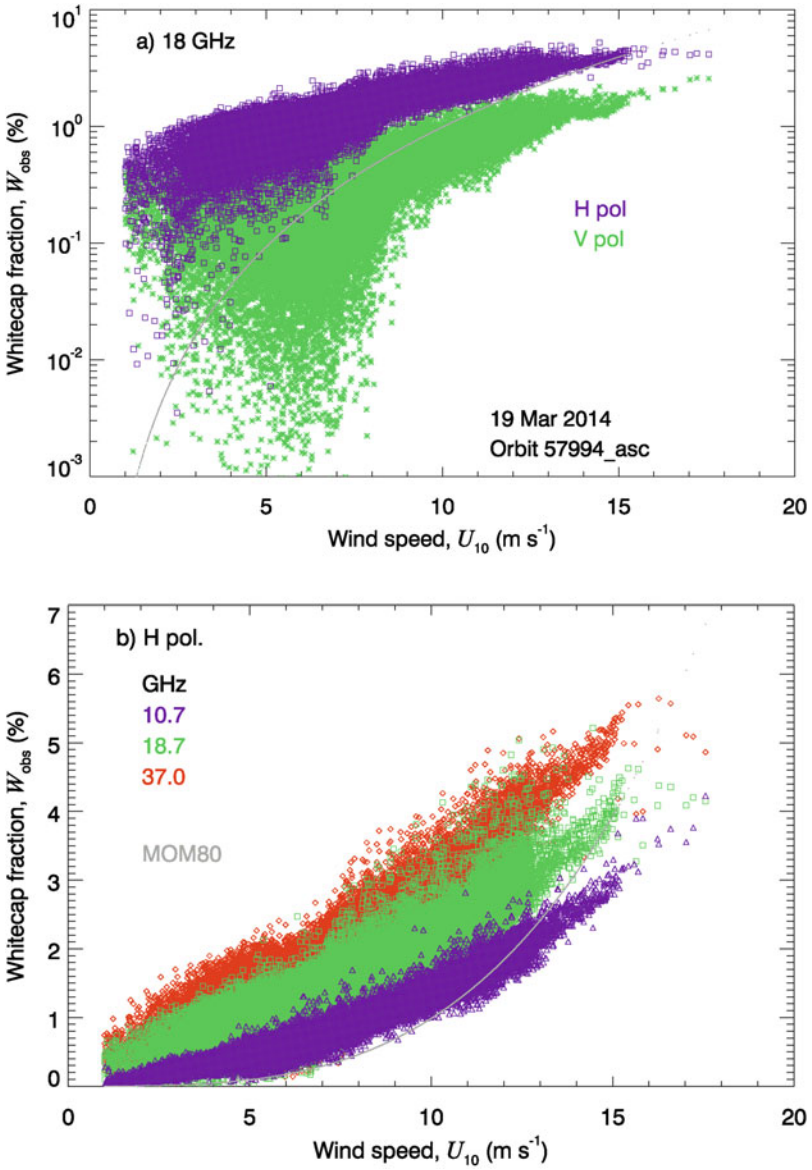

Fig. 11.1 Whitecap fraction W as a function of wind speed U_{10} obtained with the updated (latest) version of the $W(T_B)$ algorithm using WindSat retrievals as input data to models. a) W in logarithmic scale for 18 GHz, H (squares) and V (asterisks) polarizations; b) W for 10 (triangles), 18 (squares), and 37 (diamonds) GHz, H polarization in linear scale. The data are for WindSat orbit 57,994, ascending pass on 19 March 2014. The gray symbols (forming a line) are for the $W(U_{10})$ parameterization of Monahan and O'Muircheartaigh (1980, MOM80 in the legend)

The frequency and polarization variations of the radiometric W values seen in Fig. 11.1 are consistent with both measurements (Rose et al. 2002) and models (Chen et al. 2003). The frequency variations of W arise from the sensitivity of the different frequencies to the thicknesses of the foam layers (Anguelova and Gaiser 2011). Foam layers with different thicknesses provide different skin depths for emission of EM radiation, yielding different foam emissivity, thus varying T_B. These differences provide a crude way to represent whitecaps at different lifetime stages, actively breaking crests (stage A) and residual foam patches (stage B). The polarization variations (at a given frequency) are caused by different polarization sensitivity to surface roughness. The EM signals at H polarization are sensitive to both roughness and foam, and thus vary stronger with U_{10}. Conversely, the signals at V polarization are caused (presumably) mainly by the foam (V polarization is the least sensitive to roughness at $\theta \cong 53°$). These polarization differences can be helpful for tuning the $W(T_B)$ algorithm to minimize the contribution from roughness, thus to improve the retrievals of whitecap coverage.

Figure 11.2 shows global maps of W retrievals at 18 GHz (top panel) and W values obtained with the $W(U_{10})$ parametrization of Monahan and O'Muirchaertaigh (1980) (bottom panel). The data are for 19 March 2014. The comparison of the global maps shows more uniform distribution of the satellite W data from low to high latitudes compared to the one based on photographic data. This reflects the expected change of wind speed dependence due to influences of different environmental factors (Anguelova and Webster 2006; Monahan et al. 2015). The validation of the satellite W data is ongoing work (Anguelova and Bettenhausen 2019).

11.3 Whitecap Fraction Inferred from Wave Models

Until recently, the air-sea interaction community has been underutilizing wave modelling regarding whitecap fraction W. Wave modeling has been mostly called for to provide wave field characteristics for inclusion in W parameterizations. Early works proposed parameterizations of W in terms of wave spectrum (Ross and Cardone 1974; Snyder and Kennedy 1983) and wave age (Kraan et al. 1996). Numerous studies argued for explicit inclusion of wave field characteristics in the roughness length z_0 for better representation of friction velocity u_* (Donelan et al. 1993; Fairall et al. 2000; Taylor and Yelland 2001; Bourassa 2004). Accounting for the wave field via z_0 has the potential to improve $W(u_*)$ parameterizations. Parameterizations of W in terms of a (dimensionless) breaking wave parameter explicitly combine u_* with wave field characteristics such as the peak angular velocity of the wave spectrum ω_p (Zhao and Toba 2001) or H_s (Woolf 2005). Modified existing or new $W(U_{10}, etc.)$ parametrizations have used both measured or modeled data to account for the wave field (Sugihara et al. 2007; Salisbury et al. 2013; Brumer et al. 2017).

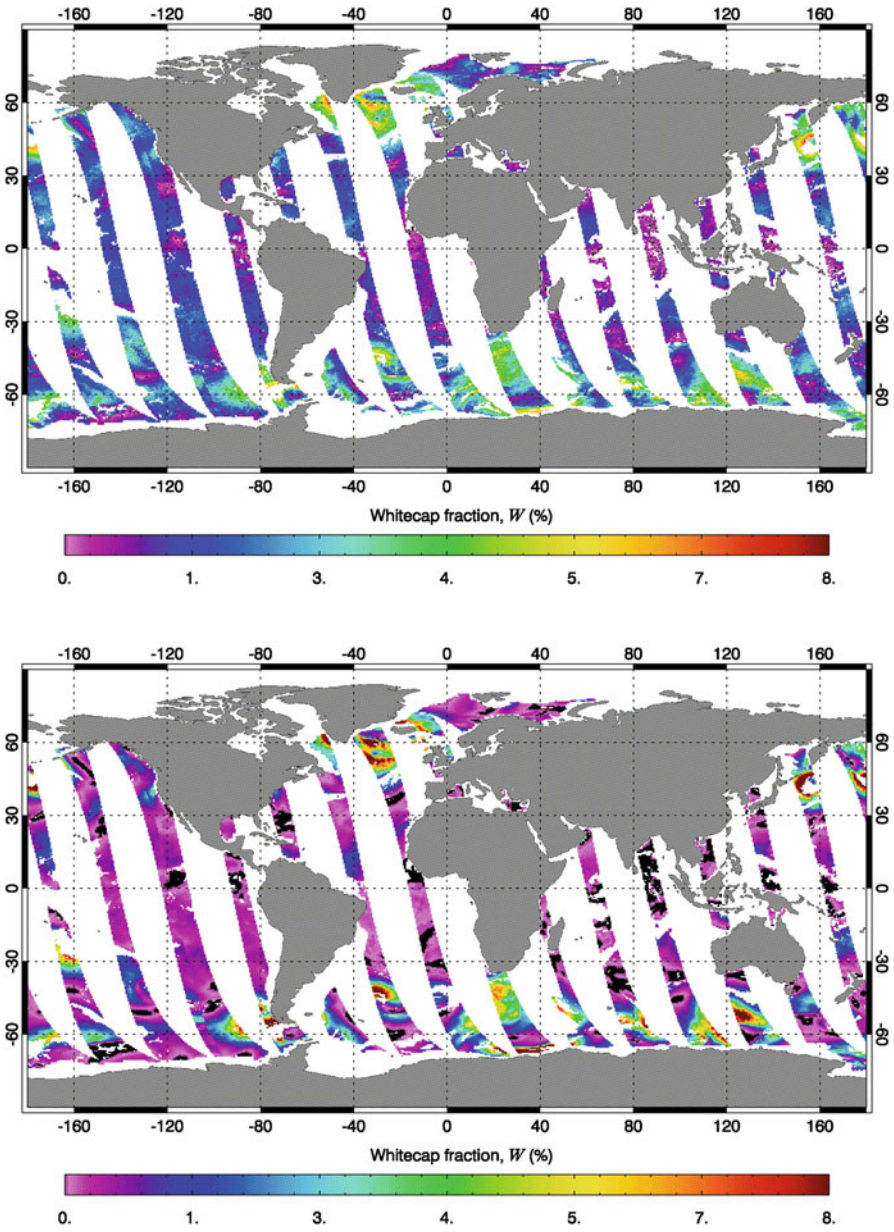

Fig. 11.2 Daily maps of whitecap fraction (19 Mar 2014): (top panel) W at 18 GHz, H polarization, obtained with the updated (latest) version of the $W(T_B)$ algorithm; (bottom panel) W from the $W(U_{10})$ parametrization of Monahan and O'Muirchaertaigh (1980) calculated with WindSat retrieval of U_{10}

Inferring (not parameterizing) W directly from wave models is a recent development. The long-standing work on including the effect of breaking wave in wave models (Komen et al. 1994; WISE Group 2007) has paved the way to this new capability. The physical basis for inferring W from wave models is the strong relationship between whitecap fraction W and the rate of energy dissipation ε. This section highlights the development and status of using wave modelling to determine whitecap fraction.

11.3.1 Breaking Waves, Energy Dissipation, and Whitecaps

Breaking waves dissipate the energy transferred from the wind to the waves. Whitecaps are the most direct, visual expression of wave breaking with air entrainment in the ocean. It is thus only logical that the two quantities that characterize the wave breaking phenomenon—namely, the rate of energy dissipation ε and the whitecap fraction W—are related. In fact, even the ubiquitous $W(U_{10})$ parameterizations originate from this $W(\varepsilon)$ relationship following the reasoning (Wu 1979, 1988, 1992):

$$W \propto \varepsilon = \tau V_c \propto \tau u_* \propto \left(C_{10}U_{10}^2\right)\left(C_{10}^{1/2}U_{10}\right) \propto U_{10}^{3.75} \tag{11.8}$$

where τ this time denotes the wind stress (not the atmospheric transmissivity as in Sect. 11.2.2), V_c is surface drift current, and C_{10} is the wind stress (or drag) coefficient.

Equation (11.8) builds on the assumption that whitecaps manifest the dissipation of excessive energy transferred from the air flow to the fully developed spectral components of the wave spectrum (Cardone 1969). This assumption contains two important notions. First, wave breaking with air entrainment is the main dissipative mechanism, thus ignoring other dissipation pathways such as microscale breaking and bottom friction (Banner and Peregrine 1993). Second, the spectral energy dissipation $S_{ds}(\omega,\theta)$ balances the spectral energy input $S_{in}(\omega,\theta)$ in the equilibrium range of the wave spectrum (Phillips 1985). This basis allows determining the total energy dissipation rate $\langle S_{ds}\rangle$ (also denoted Φ_{oc} or ε_t) of the wave field by integrating the dissipation (or the wind input) functions over wave spectrum frequency ω and direction θ (the meaning of notation θ here differs from that in Sect. 11.2.3):

$$\langle S_{ds}\rangle = \rho_w g \int_0^{2\pi}\int_0^{\infty} S_{ds}(\omega,\theta)\,d\omega\,d\theta \tag{11.9}$$

where ρ_w is the density of water and g is the acceleration due to gravity. Spectral wave models provide $S_{ds}(\omega,\theta)$. Using field data, Hwang and Sletten (2008) prove

this expected balance for the spectrally averaged terms of wind energy input $\langle S_{in} \rangle$ and wave energy dissipation $\langle S_{ds} \rangle$:

$$\langle S_{in} \rangle \cong \langle S_{ds} \rangle \tag{11.10}$$

Ross and Cardone (1974) first derived a linear expression for $W(\varepsilon)$ by combining aircraft observations of whitecaps and a simple model describing the growth of the wave spectrum due to energy transferred from a turbulent wind profile. Kraan et al. (1996) first compared W observations with W estimates from a wave model. Hanson and Phillips (1999) employed W from video records and ε computed from measured wave spectra to demonstrate that using $W(\varepsilon)$ expression reduces the range of W data scatter by 2–3 orders of magnitude compared to using $W(U_{10})$ parameterizations.

Phillips (1985) developed a theoretical framework to express W and ε in terms of breaking wave statistical properties. Phillips (1985) defined a statistical variable called breaking crest length distribution $\Lambda(\boldsymbol{c})d\boldsymbol{c}$, which quantifies the total length of breaking crests per unit area moving with a velocity in the range ($\boldsymbol{c}$, $\boldsymbol{c}$ + $d\boldsymbol{c}$) (bold letters denote vector variable). Phillips (1985) uses moments of the Λ distribution to define various breaking wave statistics. Combining the first moment of $\Lambda(\boldsymbol{c})d\boldsymbol{c}$ with the persistence time of the bubbles T_{bub}, gives the active whitecap fraction:

$$W_A = \int_c T_{bub} c \Lambda(\boldsymbol{c}) d\boldsymbol{c} \tag{11.11}$$

The fifth moment of the Λ distribution determines the energy dissipation rate:

$$\varepsilon(\boldsymbol{c})d\boldsymbol{c} \propto c^5 \Lambda(\boldsymbol{c})d\boldsymbol{c} \tag{11.12}$$

Expressions (11.10, 11.11 and 11.12) allow inferring whitecap fraction W from wave models.

11.3.2 Whitecaps from Wave Models

A full-spectral third-generation wind-wave model (WW3) uses the directional wavenumber (k) spectrum (or wave spectral energy) $F(k, \theta)$ to calculate various quantities of the wave field (WAMDI Group 1988; Komen et al. 1994; Tolman et al. 2002). Used also is the action density spectrum $N(k, \theta) = F(k, \theta)/\sigma$, where $\sigma = 2\pi f_r$ is the intrinsic radian frequency corresponding to relative frequency f_r. The wave model gives the evolution of the spectral energy in space (x, y) and time t, $F(k, \theta,$

x, y, t), using the wave energy balance equation:

$$\frac{DF}{Dt} = S_{in} + S_{nl} + S_{ds} \tag{11.13}$$

where D/Dt is the total (material) derivative and terms S are the various source and sink terms, which drive the evolution and propagation of the spectral energy F. In addition to the terms of energy input from the wind S_{in} and energy dissipation S_{ds}, the wave field is shaped by the non-linear wave-wave interaction term S_{nl}, which transfers the input energy from large to small scales.

Different wave models use different functional representations for the dissipation term S_{ds}. The spectral wave model developed by the European Center for Medium range Weather Forecasting (ECMWF), referred to as ECWAM, uses the dissipation source term of Hasselmann (1974) adjusted by Janssen et al. (1989) for proper balance at the high frequencies. It employs the total wave variance per square meter m_0 and the action density spectrum N (ECMWF 2013). The spectral wave model WAVEWATCH III, now used operationally at NOAA/NCEP (referred to as WWATCH), models S_{ds} with two contributions (Ardhuin et al. 2010), namely spontaneous dissipation $S_{sp}(k, \theta)$ that occurs when waves become steep and break, and cumulative dissipation $S_{cu}(k, \theta)$ that occurs when large-scale breakers overtake shorter waves and induce their breaking (Banner et al. 1989). The spontaneous breaking term $S_{sp}(k, \theta)$ is parameterized in terms of directional saturation spectrum $B(k, \theta)$ [i.e., related to $k^3F(k, \theta)$]. The cumulative term $S_{cu}(k, \theta)$ is parameterized in terms of Λ distribution, which, in turn, is represented with the breaking probability $P(k, \theta)$. Following Banner et al. (2002), the breaking probability is expressed via the saturation wave spectrum $B(k, \theta)$.

There are three approaches to obtain W from a spectral wave model using term S_{ds} or other functional representations.

Scanlon et al. (2016) approach relates the total energy dissipation ε_t (or Φ_{oc}) obtained with (11.10) directly to W. Following Kraan et al. (1996), Scanlon et al. (2016) assume a linear relationship between W and Φ_{oc}:

$$\langle S_{ds} \rangle \equiv \Phi_{\mathrm{oc}} = \gamma \rho_w g W \omega_p E \tag{11.14}$$

Here $E = (H_s/4)^2$ is the wave variance and factor γ represents the average fraction of total wave energy dissipated per whitecap event. Factor γ allows tuning of the results. From (11.14), W is obtained as:

$$W(\Phi_{\mathrm{oc}}) = \frac{\Phi_{\mathrm{oc}}}{\gamma \rho_w g W \omega_p E} \tag{11.15}$$

Leckler et al. (2013) approach uses Phillips (1985) concept for Λ distribution. Following Reul and Chapron (2003), the expression used is:

$$W(\Lambda) = \int_{c_{min}}^{c_p} a\lambda_c \Lambda(c) dc \tag{11.16}$$

where a is a constant and $\lambda_c = 2\pi c^2/g$ is the wavelength of the breaker. The $\Lambda(c)dc$ is converted to wavenumber form $\Lambda(k_b)dk_b$ and parameterized in terms the breaking probability $P(k)$. In addition to using it in (11.16), the $\Lambda(k_b)$ parameterization is also used to obtain the cumulative term $S_{cu}(k, \theta)$ in S_{ds}.

Anguelova and Hwang (2016) approach also uses the Phillips (1985) concept for Λ distribution. However, Anguelova and Hwang combine (11.11) and (11.12) to develop an expression for W in terms of $\varepsilon_t \equiv \langle S_{ds} \rangle$, not Λ:

$$W(\varepsilon_t) = \frac{gT}{4b\rho_w} \frac{\varepsilon_t}{c_{min}^4 \ln(c_{max}/c_{min})} \tag{11.17}$$

Here b is the breaking strength parameter (Drazen et al. 2008) and (c_{min}, c_{max}) define the range of breaking front speeds over which (11.11) is integrated. Expression (11.17) uses proper breaking statistics, but does not rely on $\Lambda(c)$ data, which are difficult to measure.

11.3.3 Modelled Whitecap Fraction

Scanlon et al. (2016) used the most recent version of ECWAM (model cycle 41R1) to obtain Φ_{oc} in (11.14) on 11-km resolution with 1-hourly output. To minimize the influence of swell-dominated sea on the W estimates, Scanlon et al. (2016) used the mean frequency $\overline{\omega}$ of the windsea part of the wave spectra instead of ω_p. The default setting of $\gamma = 0.01$ was used. The modelled W values were compared to photographically measure W values for both total (stages A + B) and active (stage A alone) whitecaps. A bias in the modeled W (positive intercept of the y axis), as compared to measured W, was minimized by introducing a threshold term in (11.15) depending on u_*:

$$W(\Phi_{oc}) = \begin{cases} \dfrac{\Phi_{oc}}{\gamma \rho_w g W \omega_p E} \left(\dfrac{u_* - u_{*T}}{u_*} \right)^3, & u_* > u_{*T} \\ 0, & u_* \le u_{*T} \end{cases} \tag{11.18}$$

where $u_{*T} = 0.065$ m s^{-1}. Tuning of the modeled W values with the γ factor also improved the comparison to measured W values. Setting $\gamma = 0.036$ and $\gamma = 0.0078$ provided the best comparisons to measured active and total W values, respectively. This γ tuning provided useful insights for the relative contributions of the active and

total whitecaps to the energy dissipation by breaking waves. The reduced γ values for the comparison to the total W data confirmed the expectation that the residual (decaying) whitecaps contribute much less to the energy transfer (from the wind to the wave to the underlying currents) than the active breaking crests.

Overall, Scanlon et al. (2016) results showed that the ECWAM dissipation term Φ_{oc} is more strongly related to the actively breaking crest (stage A whitecaps) than the mature whitecaps. Despite successful modifications as (11.18) and tuning with factor γ, the 1:1 comparison of modeled and measured W values still shows some scatter, especially at low W values. Scanlon et al. (2016) suggest that further refinement of the microscale breaking (without air entrainment) in Φ_{oc} and better account of additional metoc conditions on W may improve the modeled W values. Scanlon et al. (2016) see a great promise of providing global W data from ECWAM, which can help constrain satellite W data.

Leckler et al. (2013) used WWATCH (Sect. 11.3.2) to first compute the breaking probability $P(k)$, then $\Lambda(k_b)$, and finally obtaining $W(\Lambda)$ with (11.16). The choice of model settings (denoted TEST570 in their Table 11.1) makes the computations of the cumulative dissipation term (Sect. 11.3.2) more consistent with the spontaneous dissipation term compared to previous TEST settings. The wind speed dependence of the modeled W values compares reasonably well to that of W obtained with the $W(U_{10})$ expression of Monahan and Woolf (1989). Comparison of the WWATCH modeled W values to satellite W values obtained with the early (interim) version of the $W(T_B)$ algorithm (Sect. 11.2.3) gives larger spread. Leckler et al. (2013) attribute part of this spread to the use of ECMWF U_{10} data instead of the U_{10} data used to obtain the satellite W values. This is consistent with the analysis of Albert et al. (2016, their Sect. 3.1.2) who estimated about 5% differences in W values obtained from parametrizations using U_{10} from different sources. The 1:1 comparison of the WWATCH W data to satellite W data (Fig. 8 in Leckler et al. 2013) is better for satellite data at 10 GHz than at 37 GHz. Because satellite data at 10 GHz are more representative of active (stage A) whitecaps, this result corroborates the result of Scanlon et al. (2016) that wave models predict active W better. Leckler et al. (2013) see great advantage in modeling W for constraining the WWATCH dissipation term. Finally, Leckler et al. (2013) also see promise in the synergy between global WWATCH W data and satellite W data for further improvements of both methods.

Rogers et al. (2012) also modeled W with (11.16) using WWATCH but with TEST451 settings (Table 1 of Leckler et al. 2013). Figure 11.3 shows the calculated total dissipation term $\langle S_{ds} \rangle$ on a global scale. Rogers et al. (2012) investigated the sensitivity of S_{ds} and W calculations to the choice of the maximum prognostic frequency $f_{r\max}$ used for the S_{ds} integration. Using $f_{r\max} = 3.85$ Hz, the calculations include in the S_{ds} modeling waves as short as 10 cm; this is optimal for the S_{ds} prediction. Use of $f_{r\max} = 0.76$ Hz includes waves no shorter than 2.7 m; this may underestimate S_{ds}, especially at lower wind speeds. The results showed that the choice of $f_{r\max}$ has modest effect on $\langle S_{ds} \rangle$: the change from 0.76 Hz to 3.85 Hz increased $\langle S_{ds} \rangle$ value by 24%. However, the same change of $f_{r\max}$ increased the W values by a factor of 3.6. Modeled W values are also sensitive to the setting of constant a in (11.16). For a fixed $f_{r\max} = 0.76$ Hz, the change of a from 0.3 to 0.8

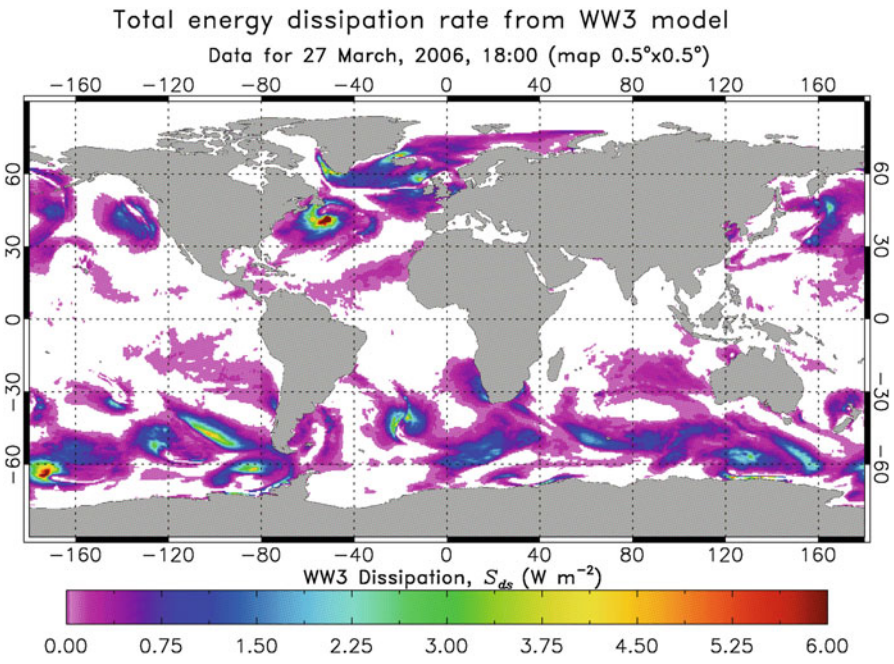

Fig. 11.3 Global map of the total energy dissipation rate from WAVEWATCH III model

increases W by a factor of 2.6. Comparison of the modeled W to satellite W (at 10 GHz) in Fig. 11.4 constrains the choice of this constant to $a = 0.3$, thus predicting W up to 5% over the globe.

Anguelova and Hwang (2016) used (11.17) to obtain W from buoy data with the parametric model of Hwang and Sletten (2008) for ε_t. However, the total dissipation in (11.17) can be obtained with other means, including the use of the wave model dissipation term $\langle S_{ds} \rangle$. Expression (11.17) is a viable alternative to both (11.15) and (11.16). On one hand, it relies solely on $\langle S_{ds} \rangle$, as in (11.15), but incorporates sound physics for the breaking statistics by virtue of its derivation from (11.11 and 11.12). On the other hand, it circumvent uncertainties in determining W caused by $\Lambda(c)$ that might be present in (11.16). Therefore, future work on using (11.17) with wave model S_{ds} is recommended.

11.4 Conclusions

The field of determining whitecap coverage W from sea state photographs, and the associated whitecap method of parameterizing air-sea fluxes of heat, gases, and sea spray, builds on the long-term, dedicate work of Dr. Edward C. Monahan. Photographic in situ measurements of W are invaluable for detail studies of air-sea

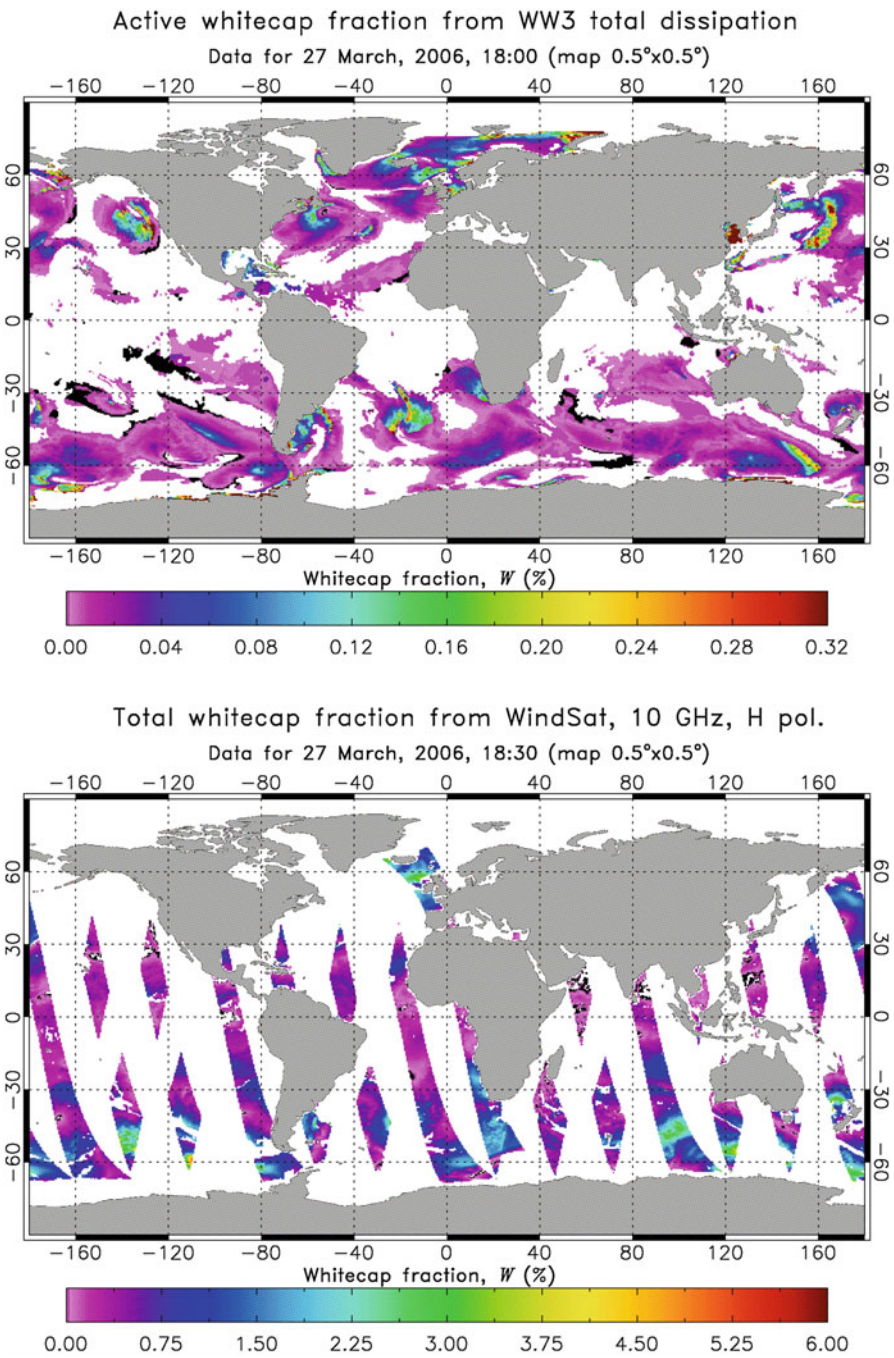

Fig. 11.4 Global maps of: (top panel) Active (stage A) whitecap fraction W from WAVEWATCH III model obtained with (11.16); (bottom panel) Predominantly active whitecap fraction W from satellite radiometric observations at 10 GHz (H polarization), obtained with early (interim) version of the $W(T_B)$ algorithm

processes. However, to improve the applicability of whitecap parametrizations to global scales, different methods need to complement the photographic W data.

Remote sensing methods at visible, infrared, and radio wavelengths and frequencies are now available to observe and measure whitecaps. Passive remote sensing of W uses brightness temperature T_B to determine W after atmospheric correction. Different versions of the $W(T_B)$ algorithm have been developed using physically sound models and various data sources as model inputs. Early versions using external data, while successful, showed wider spread of the estimated W data due to collocation mismatch. The latest version uses T_B data and model inputs from WindSat and shows improved W retrievals. Work on tuning and improving the W (T_B) algorithm is ongoing.

Inferring W from wave models shows great promise for inferring W on a global scale. The dissipation term from a wave model is used to determine W. Three different approaches of determining W are now demonstrated. Comparisons to in situ and satellite W data establish that wave models predict well the active whitecaps. The synergy between W data from satellite retreivals and wave modeling provide basis for mutual constrain and further improvements of these new methods.

Acknowledgments I am deeply grateful to Peter W. Gaiser and Richard M. Bevilacqua for unwavering support in pursuing passive remote sensing of whitecaps at Remote Sensing Division, NRL. The significant contributions of Michael H. Bettenhausen and William F. Johnston in developing the WindSat forward model and producing the WindSat data is acknowledged and highly appreciated. Credit is due to W. Erick Rogers for his work on the wave modeling. This work was sponsored by the Office of Naval Research (NRL program element 61153 N).

References

Albert, M. F. M. A., Anguelova, M. D., Manders, A. M. M., Schaap, M., & de Leeuw, G. (2016). Parameterization of oceanic whitecap fraction based on satellite observations. *Atmospheric Chemistry and Physics, 16*, 13725–13751. https://doi.org/10.5194/acp-16-13725-2016.

Anguelova, M. D. (2008). Complex dielectric constant of sea foam at microwave frequencies. *Journal of Geophysical Research, 113*, C08001. https://doi.org/10.1029/2007JC004212.

Anguelova, M. D., & Bettenhausen, M. H. (2019). Whitecap fraction from satellite measurements: Algorithm description. *Journal of Geophysical Research, 124*, 1827–1857. https://doi.org/10.1029/2018JC014630.

Anguelova, M. D., & Gaiser, P. W. (2011). Skin depth at microwave frequencies of sea foam layers with vertical profile of void fraction. *Journal of Geophysical Research, 116*, C11002. https://doi.org/10.1029/2011JC007372.

Anguelova, M. D., & Gaiser, P. W. (2012). Dielectric and radiative properties of sea foam at microwave frequencies: Conceptual understanding of foam emissivity. *Remote Sensing, 4*, 1162–1189. https://doi.org/10.3390/rs4051162.

Anguelova, M. D., & Gaiser, P. W. (2013). Microwave emissivity of sea foam layers with vertically inhomogeneous dielectric properties. *Remote Sensing of Environment, 139*, 81–96. https://doi.org/10.1016/j.rse.2013.07.017.

Anguelova, M. D., & Hwang, P. A. (2016). Using energy dissipation rate to obtain active whitecap fraction. *Journal of Physical Oceanography, 46*, 461–481. https://doi.org/10.1175/JPO-D-15-0069.1.

Anguelova, M. D., & Webster, F. (2006). Whitecap coverage from satellite measurements: A first step toward modeling the variability of oceanic whitecaps. *Journal of Geophysical Research, 111*, C03017. https://doi.org/10.1029/2005JC003158.

Ardhuin, F., Rogers, E., Babanin, A., Filipot, J.-F., Magne, R., Roland, A., van der Westhuysen, A., Queffeulou, P., Lefevre, J.-M., Aouf, L., & Collard, F. (2010). Semi-empirical dissipation source functions for ocean waves: Part I, definitions, calibration and validations. *Journal of Physical Oceanography, 40*, 1917–1941.

Asher, W. E., et al. (1995). Measurement of gas transfer, whitecap coverage, and brightness temperature in a surf pool: An overview of WABEX-93. In B. Jähne & E. Monahan (Eds.), *Air-water gas transfer* (pp. 205–216). Hanau: AEON Verlag.

Asher, W. E., Wang, Q., Monahan, E. C., & Smith, P. M. (1998). Estimation of air--sea gas transfer velocities from apparent microwave brightness temperature. *Marine Technology Society Journal, 32*, 32–40.

Banner, M. L., Jones, I. S. F., & Trinder, J. C. (1989). Wavenumber spectra of short gravity waves. *Journal of Fluid Mechanics, 198*, 321–344. https://doi.org/10.1017/S0022112089000157.

Banner, M. L., Gemmrich, J. R., & Farmer, D. M. (2002). Multiscale measurement of ocean wave breaking probability. *Journal of Physical Oceanography, 32*, 3364–3374.

Banner, M. L., & Peregrine, D. H. (1993). Wave breaking in deep water. *Annual Review of Fluid Mechanics, 25*(1), 373–397. https://doi.org/10.1146/annurev.fl.25.010193.002105.

Bettenhausen, M. H., Smith, C .K., Bevilacqua, R. M., Wang, N.–Y., Gaiser, P. W., and Cox, S. (2006). A nonlinear optimization algorithm for WindSat wind vector retrievals. Transactions on Geoscience and Remote Sensing, 44(3), 597–610. https://doi.org/10.1109/TGRS.2005.862504.

Bobak, J. P., Asher, W. E., Dowgiallo, D. J., & Anguelova, M. D. (2011). Aerial radiometric and video measurements of whitecap coverage. *Transactions on Geoscience and Remote Sensing, 49*(6), 2183–2193. https://doi.org/10.1109/TGRS.2010.2103565.

Bondur, V., & Sharkov, E. (1982). Statistical properties of whitecaps on a rough sea. *Oceanology, 22*, 274–279.

Bourassa, M. (2004). An improved sea state dependency for surface stress derived from in situ and remotely sensed winds. *Advances in Space Research, 33*, 1136–1142.

Brumer, S. E., Zappa, C. J., Brooks, I. M., Tamura, H., Brown, S. M., Blomquist, B. W., Fairall, C. W., & Cifuentes-Lorenzen, A. (2017). Whitecap coverage dependence on wind and wave statistics as observed during SO GasEx and HiWinGS. *Journal of Physical Oceanography, 47*, 2211–2235. https://doi.org/10.1175/JPO-D-17-0005.1.

Cardone, V. J. (1969). *Specification of the wind distribution in the marine boundary layer for wave forecasting* (Tech. Rep. 69–1, Geophys) (131 pp). Sci. Lab: New York University.

Chen, D., Tsang, L., Zhou, L., Reising, S. C., Asher, W. E., Rose, L. A., Ding, K. H., & Chen, C. T. (2003). Microwave emission and scattering of foam based on Monte Carlo simulations of dense media. *IEEE Transactions on Geoscience and Remote Sensing, 41*, 782–790.

de Leeuw, G., Andreas, E. L , Anguelova, M. D., Fairall, C. W., Lewis, E. R., O'Dowd, C. D., Schulz, M., and Schwartz, S. E. (2011). Production flux of sea-spray aerosol. Reviews of Geophysics, 49, RG2001. https://doi.org/10.1029/2010RG000349.

Donelan, M., Dobson, F., Smith, S., & Anderson, R. (1993). On the dependence of sea surface roughness on wave development. *Journal of Physical Oceanography, 23*, 2143–2149.

Drazen, D. A., Melville, W. K., & Lenain, L. (2008). Inertial scaling of dissipation in unsteady breaking waves. *Journal of Fluid Mechanics, 611*, 307332. https://doi.org/10.1017/S0022112008002826.

Droppleman, J. (1970). Apparent microwave emissivity of sea foam. *Journal of Geophysical Research, 75*, 696–698.

ECMWF. (2013). *IFS documentation CY40r1, Part VII: ECMWF Wave Model*. ECMWF Model Doc., 79 p., http://www.ecmwf.int/sites/default/files/IFS_CY40R1_Part7.pdf

Fairall, C., Hare, J., Edson, J., & McGillis, W. (2000). Parameterization and micrometeorological measurement of Air–Sea gas transfer. *Boundary-Layer Meteorology, 96*, 63–106.

Gaiser, P. W., St Germain, K. M., Twarog, E. M., Poe, G. A., Purdy, W., Richardson, D., et al. (2004). The WindSat spaceborne polarimetric microwave radiometer: Sensor description and early orbit performance. *Transactions on Geoscience and Remote Sensing, 42*, 2347–2361. https://doi.org/10.1109/TGRS.2004.836867.

Goddijn-Murphy, L., Woolf, D. K., & Callaghan, A. H. (2011). Parameterizations and algorithms for oceanic whitecap coverage. *Journal of Physical Oceanography, 41*, 742–756.

Hanson, J. L., & Phillips, O. M. (1999). Wind sea growth and dissipation in the open ocean. *Journal of Physical Oceanography, 29*, 1633–1648.

Hasselmann, K. (1974). On the spectral dissipation of ocean waves due to whitecapping. *Boundary-Layer Meteorology, 6*, 107–127.

Hwang, P. A., & Sletten, M. A. (2008). Energy dissipation of wind-generated waves and whitecap coverage. *Journal of Geophysical Research, 113*, C02012. https://doi.org/10.1029/2007JC004277. (Corrigendum 2009, 114, C02015. https://doi.org/10.1029/2008JC005244).

Janssen, P. A. E. M., Lionello, P., Reistad, M., & Hollingsworth, A. (1989). Hindcasts and data assimilation studies with the WAM model during the Seasat period. *Journal of Geophysical Research, C94*, 973–993.

Jessup, A. T., Zappa, C. J., Loewen, M. R., & Hesany, V. (1997). Infrared remote sensing of breaking waves. *Nature, 385*, 52–55.

Komen, G. J., Cavaleri, L., Donelan, M., Hasselmann, K., Hasselmann, S., & Janssen, P. A. E. M. (1994). *Dynamics and modeling of ocean waves* (532 pp). Cambridge: Cambridge University Press.

Kraan, C., Oost, W., & Janssen, P. (1996). Wave energy dissipation by whitecaps. *Journal of Atmospheric and Oceanic Technology, 13*, 262–267.

Leckler, F., Ardhuin, F., Filipot, J. F., & Mironov, A. (2013). Dissipation source terms and whitecap statistics. *Ocean Modelling, 70*(2013), 62–74. https://doi.org/10.1016/j.ocemod.2013.03.007.

Meissner, T., & Wentz, F. J. (2012). The emissivity of the ocean surface between 6 and 90 GHz over a large range of wind speeds and earth incidence angles. *Transactions on Geoscience and Remote Sensing, 50*(8), 3004–3026. https://doi.org/10.1109/TGRS.2011.2179662.

Melville, W., & Matusov, P. (2002). Distribution of breaking waves at the ocean surface. *Nature, 417*, 58–63.

Militskii, Y. A., Raizer, V. Y., Sharkov, E. A., & Etkin, V. S. (1978). Thermal radio emission from foam structures. *Soviet Physics – Technical Physics, 23*, 601–602.

Mironov, A. S., & Dulov, V. A. (2008). Detection of wave breaking using sea surface video records. *Measurement Science and Technology, 19*, 015405. https://doi.org/10.1088/0957-0233/19/1/015405.

Monahan, E. C. (1971). Oceanic whitecaps. *Journal of Physical Oceanography, 1*, 139–144.

Monahan, E. C., Hooker, G., Zappa, C. J. (2015). The latitudinal variation in the wind-speed parameterization of oceanic whitecap coverage; implications for global modelling of air-sea gas flux and sea surface aerosol generation. In: *19th Conference on Air-Sea Interaction, January 04–08, Phoenix, AZ.*

Monahan, E. C., & Lu, M. (1990). Acoustically relevant bubble assemblages and their dependence on meteorological parameters. *Journal of Oceanic Engineering, 15*(4), 340–349. https://doi.org/10.1109/48.103530.

Monahan, E. C., & O'Muircheartaigh, I. (1980). Optimal power-law description of oceanic whitecap coverage dependence on wind speed. *Journal of Physical Oceanography, 10*, 2094–2099. https://doi.org/10.1175/1520-0485(1980)010<2094:OPLDOO>2.0.CO;2.

Monahan, E. C., & O'Muircheartaigh, I. (1986). Whitecaps and the passive remote sensing of the ocean surface. *International Journal of Remote Sensing, 7*, 627–642. https://doi.org/10.1080/01431168608954716.

Monahan, E. C., & Woolf, D. K. (1989). Comments on variations of whitecap coverage with wind stress and water temperature. *Journal of Physical Oceanography, 19*, 706–709.

Nordberg, W., Conaway, J., Ross, D., & Wilheit, T. (1971). Measurements of microwave emission from a foam-covered, wind-driven sea. *Journal of the Atmospheric Sciences*, *28*, 429–435.

Padmanabhan, S., Reising, S. C., Asher, W. E., Rose, L. A., & Gaiser, P. W. (2006). Effects of foam on ocean surface microwave emission inferred from radiometric observations of reproducible breaking waves. *IEEE Transactions on Geoscience and Remote Sensing, 44*, 569–583.

Paget, A. C., Bourassa, M. A., & Anguelova, M. D. (2015). Comparing in situ and satellite-based observations of oceanic whitecaps. *Journal of Geophysical Research, 120*, 2826–2843. https://doi.org/10.1002/2014JC010328.

Pandey, P., & Kakar, R. (1982). An empirical microwave emissivity model for a foam-covered sea. *Journal of Oceanic Engineering, 7*(3), 135–140. https://doi.org/10.1109/JOE.1982.1145527.

Phillips, O. M. (1985). Spectral and statistical properties of the equilibrium range in wind-generated gravity-waves. *Journal of Fluid Mechanics, 156*, 505–531.

Potter, H., Smith, G. B., Snow, C. M., Dowgiallo, D. J., Bobak, J. P., & Anguelova, M. D. (2015). Whitecap lifetime stages from infrared imagery with implications for microwave radiometric measurements of whitecap fraction. *Journal of Geophysical Research, 120*, 7521–7537. https://doi.org/10.1002/2015JC011276.

Randolph, K., Dierssen, H. M., Cifuentes-Lorenzen, A., Balch, W., Monahan, E. C., Zappa, C., Drapeau, D., & Bowler, B. (2017). Novel methods for optically measuring whitecaps under natural wave breaking conditions in the Southern Ocean. *Journal of Atmospheric and Oceanic Technology, 34*, 533–554. https://doi.org/10.1175/JTECH-D-16-0086.1.

Reul, N., & Chapron, B. (2003). A model of sea-foam thickness distribution for passive microwave remote sensing applications. *Journal of Geophysical Research, 108*(C10), 3321. https://doi.org/10.1029/2003JC001887.

Rogers, W. E., Anguelova, M. D., Hwang, P. A. (2012). *Satellite radiometer (Windsat) estimates of whitecap coverage interpreted using a global numerical wave model hindcast*. Abstract OS13E-1780 presented at 2012 fall meeting, AGU, San Francisco, Calif., 3–7 Dec.

Rose, L. A., Asher, W. E., Reising, S. C., Gaiser, P. W., St Germain, K. M., Dowgiallo, D. J., Horgan, K. A., Farquharson, G., & Knapp, E. J. (2002). Radiometric measurements of the microwave emissivity of foam. *IEEE Transactions on Geoscience and Remote Sensing, 40*, 2619–2625.

Ross, D., & Cardone, V. (1974). Observations of oceanic whitecaps and their relation to remote measurements of surface wind speed. *Journal of Geophysical Research, 79*, 444–452.

Salisbury, D. J., Anguelova, M. D., & Brooks, I. M. (2013). On the variability of whitecap fraction using satellite-based observations. *Journal of Geophysical Research, 118*, 6201–6222. https://doi.org/10.1002/2013JC008797.

Scanlon, B., Breivik, Ø., Bidlot, J.-R., Janssen, P., Callaghan, A., & Ward, B. (2016). Modelling whitecap coverage with a wave model. *Journal of Physical Oceanography, 46*, 887–894. https://doi.org/10.1175/JPO-D-15-0158.1.

Smith, P. M. (1988). The emissivity of sea foam at 19 and 37 GHz. *IEEE Transactions on Geoscience and Remote Sensing, 26*, 541–547.

Snyder, R., & Kennedy, R. (1983). On the formation of whitecaps by a threshold mechanism. Part I: Basic formalism. *Journal of Physical Oceanography, 13*, 1482–1492.

Stogryn, A. P. (1967). The apparent temperature of the sea at microwave frequencies. *Transactions on Antennas and Propagation, 15*(2), 278–286. https://doi.org/10.1109/TAP.1967.1138900.

Stogryn, A. P. (1972). The emissivity of sea foam at microwave frequencies. *Journal of Geophysical Research, 77*(9), 1658–1666. https://doi.org/10.1029/JC077i009p01658.

Sugihara, Y., Tsumori, H., Ohga, T., Yoshioka, H., & Serizawa, S. (2007). Variation of whitecap coverage with wave-field conditions. *Journal of Marine Systems, 66*, 47–60. https://doi.org/10.1016/j.jmarsys.2006.01.014.

Taylor, P., & Yelland, M. (2001). The dependence of sea surface roughness on the height and steepness of the waves. *Journal of Physical Oceanography, 31*, 572–590.

Tolman, H. L., Balasubramaniyan, B., Burroughs, L. D., Chalikov, D. V., Chao, Y. Y., Chen, H. S., & Gerald, V. M. (2002). Development and implementation of wind-generated ocean surface wave models at NCEP. *Weather Forecasting, 17*, 311–333. https://doi.org/10.1175/1520-0434(2002)017,0311:DAIOWG.2.0.CO;2.

WAMDI Group. (1988). The WAM model—A third generation ocean wave prediction model. *Journal of Physical Oceanography, 18*, 1775–1810. https://doi.org/10.1175/1520-0485(1988)018,1775:TWMTGO.2.0.CO;2.

Wang, Q., Monahan, E., Asher, W., & Smith, P. (1995). Correlations of whitecap coverage and gas transfer velocity with microwave brightness temperature for plunging and spilling breaking waves. In B. Jähne & E. Monahan (Eds.), *Air-water gas transfer* (pp. 217–225). Hanau: AEON Verlag.

Wentz, F. J. (1975). A two-scale scattering model for foam-free sea microwave brightness temperatures. *Journal of Geophysical Research, 80*(24), 3441–3446. https://doi.org/10.1029/JC080i024p03441.

Wentz, F. J. (1983). A model function for ocean microwave brightness temperatures. *Journal of Geophysical Research, 88*(C3), 1892–1908. https://doi.org/10.1029/JC088iC03p01892.

Wentz, F. J. (1997). A well-calibrated ocean algorithm for special sensor microwave/imager. *Journal of Geophysical Research, 102*(C4), 8703–8718. https://doi.org/10.1029/96JC01751.

Williams, G., Jr. (1969). Microwave radiometry of the ocean and the possibility of marine wind velocity determination from satellite observations. *Journal of Geophysical Research, 18*, 4591–4594.

WISE Group. (2007). *Progress in Oceanography, 75*, 603–674. https://doi.org/10.1016/j.pocean.2007.05.005.

Woolf, D. K. (2005). Parametrization of gas transfer velocities and sea-state-dependent wave breaking. *Tellus, 57B*, 87–94.

Wu, J. (1979). Oceanic whitecaps and sea state. *Journal of Physical Oceanography, 9*, 1064–1068.

Wu, J. (1988). Variations of whitecap coverage with wind stress and water temperature. *Journal of Physical Oceanography, 18*, 1448–1453.

Wu, J. (1992). Individual characteristics of whitecaps and volumetric description of bubbles. *IEEE Transactions on Antennas and Propagation, 17*, 150–158.

Zhao, D., & Toba, Y. (2001). Dependence of whitecap coverage on wind and wind-wave properties. *Journal of Oceanography, 57*, 603–616.